Oxygen and strontium codoping of La$_2$NiO$_4$:   Room-temperature phase diagrams

M. Hücker,[1] K. Chung,[2] M. Chand,[2] T. Vogt,[1] J. M. Tranquada,[1] and D. J. Buttrey[2]

[1]*Physics Department, Brookhaven National Laboratory, Upton, New York 11973, USA*

[2]*Department of Chemical Engineering, University of Delaware, Newark, Delaware 19716, USA*

We present a detailed room-temperature x-ray powder diffraction study on La$_{2-x}$Sr$_x$NiO$_{4+\delta}$ with $0 \leqslant x \leqslant 0.12$ and $0 \leqslant \delta \leqslant 0.13$. For $x=0.02$, 0.04, and 0.06 the oxygen content phase diagrams of the Sr-doped samples show a similar sequence of pure phases and miscibility gaps as for pure La$_2$NiO$_{4+\delta}$. We find a weak Sr-doping dependence of the δ range for the pure low-temperature orthorhombic (LTO), low-temperature tetragonal, and high-temperature tetragonal (HTT) phases, but overall, the δ ranges of the different phases do not vary strongly for $x \leqslant 0.06$. Drastic changes are observed for $x=0.08$ and 0.12, where miscibility gaps successively disappear. For $x=0.12$ all oxygen-doped samples are in the HTT phase. The mechanism responsible for the suppression of the phase separation seems to involves multiple factors, including the Coulomb interaction between Sr impurities and interstitial oxygens as well as the reduction of the NiO$_6$ octahedral tilt angle. The doping dependence of the lattice parameters shows clear differences for pure Sr and pure O doping. With the exception of the LTO phase, the in-plane lattice parameters explicitly depend on the type of dopant, rather than the net hole content $p=x+2\delta$. In contrast, the orthorhombic strain in the LTO phase as well as the c-axis length appears to depend only on p, however, in the case of the c-axis length this "universal" behavior turns out to be coincidental. Our results also show that the chemical pressure of La-site dopants is highly anisotropic, whereas that of O interstitials appears to be more isotropic. In general, this study reveals that for an investigation of the intrinsic properties of La$_{2-x}$Sr$_x$NiO$_4$ with $x \leqslant 0.12$, samples have to be annealed carefully to achieve $\delta=0$, since already an excess oxygen content as small as $\delta=0.01$ leads to phase separation.

I. INTRODUCTION

In recent years La$_{2-x}$Sr$_x$NiO$_{4+\delta}$ (Refs. 1–4) has been studied intensively because of its close relationship with the isostructural high-T_c superconductor La$_{2-x}$Sr$_x$CuO$_{4+\delta}$.[5–7] In both systems the transition-metal-oxide planes (NiO$_2$, CuO$_2$) can be doped with holelike charge carriers resulting in a large number of different structural and electronic phases, in particular the superconducting phase in the case of the cuprates. Although the nickelate system does not exhibit superconductivity, its investigation is very helpful to understand many features of the cuprates, such as oxygen phase separation[5,8–10] and stripe correlations.[6,11,12] Nickelates are quite amenable to study for several reasons: (1) high x and δ can be reached, (2) it is much easier to obtain homogeneously oxygen-charged samples, and (3) stripe correlations are more stable and therefore easier to detect than in the cuprates. In most experiments the intention is to introduce holes either by Sr substitution (x) or by excess oxygen (δ). However, as-grown Sr-doped nickelates frequently contain a considerable amount of excess oxygen, which can have a strong impact on various properties. Lack of knowledge of δ can lead to misinterpretations of properties of these materials.

Substitution of Sr^{2+} for La^{3+} appears to be random and has a relatively weak effect on the lattice. The phase diagram of La$_{2-x}$Sr$_x$NiO$_4$ in Fig. 1(a) shows four structural phases: a high-temperature tetragonal (HTT) phase, a low-temperature orthorhombic (LTO) phase, a low-temperature less orthorhombic (LTO2) phase, and a low-temperature tetragonal (LTT) phase; for details see Sec. III B.[13] At room temperature the structure changes at $x \simeq 0.12$ from the LTO to the HTT phase, mainly due to the decrease of the sublattice mismatch between the (La,Sr)-O and the Ni-O bond lengths with increasing hole content.

Excess oxygen occupies interstitial lattice sites centered within the LaO bilayers[14] and results in the formation of several structurally and compositionally distinct phases separated by miscibility gaps.[1,4] The O-doping phase diagram has been studied by several groups with different techniques.[1,2,4,15–18] Though there are some discrepancies between the various proposed phase diagrams, most features are captured by our schematic diagram in Fig. 1(b).[4] As a function of δ, at room temperature the system shows a sequence of pure phases LTO$\rightarrow$LTT$\rightarrow$HTT separated by biphasic regions of LTO/LTT and LTT/HTT. These biphasic regions are the result of miscibility gaps which follow from the unmixing of interstitial oxygen defects into oxygen-poor and oxygen-rich domains. The oxygen-poor domains take the maximum δ value of the bordering pure low-δ phase and the oxygen-rich domains the minimum δ of the pure high-δ phase. Strong interstitial oxygen correlations give rise to these miscibility gaps. For moderate oxygen concentrations the HTT phase transforms into a phase with one-dimensional (1D) stage order of the oxygen interstitials upon cooling below room temperature.[4] Onset of staged ordering may involve opening of additional miscibility gaps or intergrowth of stacking faults in the staging sequence, allowing for variation in average oxygen stoichiometry throughout this compositional range.[4] Finally, at very high δ three-dimensional (3D) oxygen order is observed.[25–27]

In La$_2$NiO$_4$, the NiO$_2$ planes form a two-dimensional (2D) spin $S=1$ Heisenberg antiferromagnet (AF) on a square
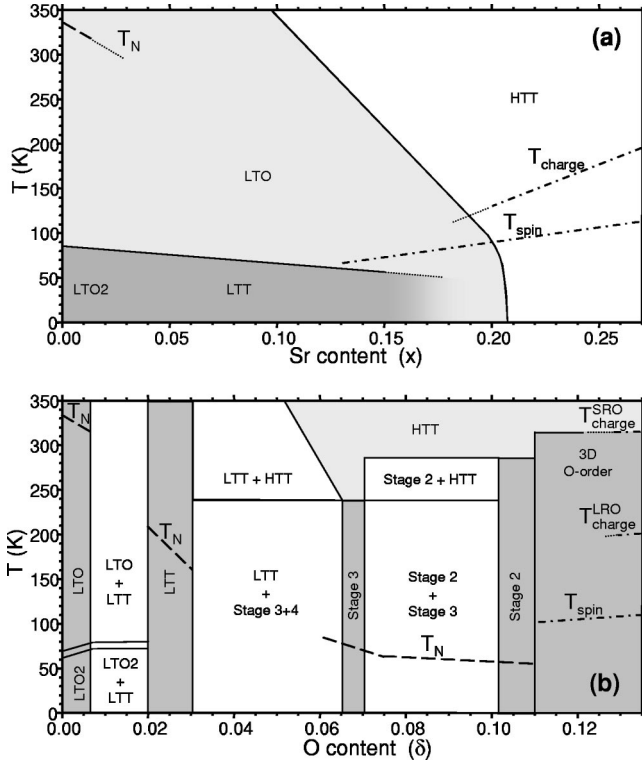
FIG. 1. Schematic phase diagram of (a) $La_{2-x}Sr_xNiO_4$ (after Refs. 19–22 and this work) and (b) $La_2NiO_{4+\delta}$ (after Refs. 1, 4, 23, and 24). In (b) we neglect that the miscibility gap boundaries near the upper consolutes are rounded. The dotted lines in both diagrams indicate unknown phase boundaries. SRO and LRO are standing for short- and long-range order, respectively.

lattice, with a Néel temperature of ~ 330 K.[28,29] As the system is doped with an increasing concentration of holes $p = x + 2\delta$, the commensurate AF order is destroyed and a phase of static charge and spin stripes forms. The stripe phase is the consequence of an electronic phase separation into hole-rich charge stripes acting as antiphase boundaries between hole-poor AF spin stripes.[12] So far, for pure Sr doping stripe order has been observed for hole concentrations $p = x \gtrsim 0.135$ and in the case of O doping for $p = 2\delta \gtrsim 0.22$ (see Fig. 1).[3,20,27,30] In the latter case, the first appearance of stripe order might be connected to that of the 3D order of the O interstitials.[23,24,30]

The idea of an interplay between the electronic phase separation in the NiO_2 planes, the structural phase separations, and the O interstitial ordering within the rocksalt bilayers has been a strong motivating factor behind this work. We are interested in the question of how additional doping by Sr affects the various phases and phase boundaries of the oxygen-content phase diagram. In particular, are the observed phases the result of purely steric effects of the interstitials or are they partially stabilized by electronic correlations? Beyond these questions it is desirable to map the structural phase diagram of (Sr,O)-codoped La_2NiO_4 so that in future, for a particular Sr content, the δ value of the sample can be determined simply by measuring its lattice parameters.

In the present paper, our focus is on the study of specimens with fixed Sr concentrations in the range $0.02 \leqslant x$

$\leqslant 0.12$ and variable interstitial oxygen concentrations in the range $0 \leqslant \delta \leqslant 0.13$ at room temperature. Phase separation into oxygen-poor and -rich domains similar to $x = 0$ was observed for all $x \leqslant 0.06$. Drastic changes occur only for the higher Sr concentrations $x = 0.08$ and 0.12, where first the LTT/HTT miscibility gap and then also the LTO/LTT miscibility gap disappears. At such high Sr concentrations the angle of the coherent octahedral tilts, with respect to $x = 0$, is already considerably reduced and finally becomes zero for $x = 0.12$. Our results rely on a precise adjustment of δ, which we have accomplished by controlled atmosphere annealing under conditions of temperature and oxygen fugacity that depend on x.[31] In fact, we find that for all samples with $x \leqslant 0.08$ an excess oxygen concentration smaller than $\delta = 0.01$ is sufficient to induce an unmixing into oxygen-poor and oxygen-rich phases. Hence, to study the intrinsic properties of $La_{2-x}Sr_xNiO_4$ the oxygen content δ has to be zero, or at least $\leqslant 0.01$. We compare our data with results for $La_{2-x}Sr_xNiO_4$ prepared in air, Ca- and Ba-doped La_2NiO_4, $Pr_2NiO_{4+\delta}$, and $Pr_{2-x}Sr_xNiO_4$.[32–34]

II. EXPERIMENTAL

Several series of $La_{2-x}Sr_xNiO_{4+\delta}$ powder samples with fixed Sr content (x) and variable excess oxygen content (δ) have been prepared. The starting crystals with $x = 0$, 0.02, 0.04, 0.06, 0.08, and 0.12 were obtained by congruent melt growth using radio frequency induction skull melting.[35] All samples crystalized in the T phase, i.e., no impurity phases were detected. Note that the interstitial oxygen phase separation occurs by unmixing from a higher-temperature single phase parent. The resulting biphasic mixtures should not be confused with impurity phases as they are intrinsic. To adjust δ, small crystal pieces were annealed at different temperatures in atmospheres with different oxygen fugacities f_{O_2} ranging from $\log_{10}(f_{O_2}) = -12$ to 0. Samples with low δ were obtained by anneals at 1000 °C and different f_{O_2}. Samples with medium and high δ were obtained by anneals at 900, 750, 600, and 450 °C in Ar and pure O_2, respectively. The oxygen fugacity was monitored electrochemically using a Y-stabilized ZrO_2 cell against a 1 atm O_2 reference. All anneals were terminated by a quench to room temperature. The oxygen content was determined by iodometric titration. Details of crystal growth, O annealing, and chemical analysis are described in Refs. 1, 33, and 36–38. Synchrotron x-ray powder diffraction patterns at room temperature were collected at beamline X7A of the National Synchrotron Light Source at Brookhaven using a Ge(111) monochromator at wavelengths λ of 0.66, 0.7, or 0.8 Å. Photons were collected with a position-sensitive detector.[39] Spectra were typically acquired in the range $10° < 2\theta < 50°$ by measuring in 0.25° steps for 30 to 60 sec per step. Powder samples were contained in glass capillaries (⌀0.4 mm) sealed under argon. To avoid potential long-term exposure to oxygen between annealing and measurement, capillaries were stored under mineral oil.

III. RESULTS

A. Excess oxygen content δ vs $2c/(a+b)$

Essential for this study is the precise knowledge of δ for each specimen. In Fig. 2 we show the iodometrically deter-
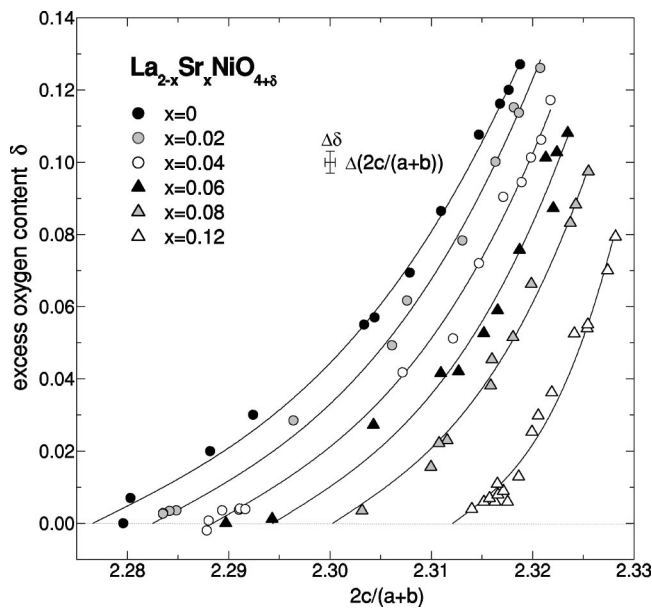
FIG. 2. Excess oxygen content δ in La$_{2-x}$Sr$_x$NiO$_{4+\delta}$ for samples with fixed Sr content $x=0$, 0.02, 0.04, 0.06, 0.08, 0.12 as a function of $2c/(a+b)$. Solid lines are fits to the data (see text). The error bars indicate the experimental error in δ and $2c/(a+b)$. The data for $x=0$ and $\delta \leqslant 0.055$ are taken from Ref. 1

FIG. 3. Crystal structure of La$_{2-x}$Sr$_x$NiO$_4$. (a) K$_2$NiF$_4$ unit cell of HTT phase with lattice constants and basis vectors of $\sqrt{2}a \times \sqrt{2}b \times c$ supercell. (b) and (c) Octahedral tilt directions in the LTO and LTT phases.

mined δ values for the various sample series with fixed x as a function of $2c/(a+b)$ determined by x-ray diffraction. All samples in this diagram are single phase, since only for these samples δ can be connected to a unique value of $2c/(a+b)$. In the case of biphasic samples, the iodometrically determined δ corresponds to the average oxygen content of the sample, which is not representative of either of the two phases. Hence, data for biphasic samples are not included in this diagram. Iodometric analysis were performed in triplicate under an inert atmosphere using deaerated solutions and standardized thiosulfate solutions.[1,36–38] Within each of these series, δ increases super-linearly as a function of $2c/(a+b)$. With increasing x, curves are shifted systematically to higher $2c/(a+b)$. Anneals performed under the same conditions with specimens of different x show a systematic decrease in δ with increasing x. The absolute random errors of δ and $2c/(a+b)$ were determined to be ± 0.003 and ± 0.0005, respectively. Note, that the relative error of $2c/(a+b)$ ($\pm 0.02\%$) is much smaller than those of a, b, and c ($\pm 0.1\%$), since certain errors, as for example that from uncertainties in λ, cancel out in the ratio. To smooth and interpolate the results, we have applied empirical least-squares fits, indicated by the solid lines, to the δ vs $2c/(a+b)$ data. Values of δ evaluated from these curves using the measured $2c/(a+b)$ were subsequently used to plot other quantities as a function of δ or $p=x+2\delta$. The fits, shown in Fig. 2 as solid lines, are power laws up to 3rd order, and were fitted simultaneously for all x. The coefficients of the nonlinear terms were varied independently for each curve. The coefficient of the linear term, i.e., the initial slope at $\delta=0$, as well as the value of $2c/(a+b)$ at $\delta=0$, were allowed to vary linearly as a function of x. Uncertainties in δ versus $2c/(a+b)$ are primarily due to the limited mass of sample
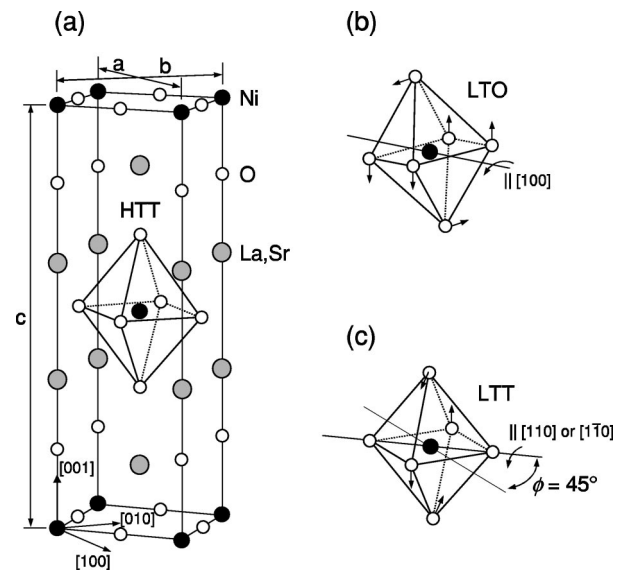
used for the individual titrations of large numbers of specimens. In the future, we plan to characterize this relationship more carefully using larger specimens. This is expected to also reveal any fine structure that may be obscured in the fits provided here.

B. Distinction of structural phases

At high temperatures La$_{2-x}$Sr$_x$NiO$_{4+\delta}$ is expected to have the ideal K$_2$NiF$_4$ HTT structure (space group $I4/mmm$) regardless of the oxygen stoichiometry [see Fig. 3(a)]. The crystal lattice consists of NiO$_2$ monolayers separated by (La,Sr)O rocksalt bilayers. Each Ni site is coordinated by six oxygens, resulting in a network of corner-sharing NiO$_6$ octahedra. The formal valence of the NiO$_2$ planes is negative while that of the (La,Sr)O bilayers is positive. Doping with interstitial oxide ions or Sr^{2+} reduces the positive net charge in the rocksalt bilayers. Similarly, the compensating holes serve to reduce the negative net charge in the NiO$_2$ planes. Overall, doping decreases the charge separation inherent to the structure, providing a stabilizing effect.

With decreasing temperature different structural transitions are observed depending on x and δ. Most of these low temperature phases can be described by different patterns of slightly tilted, almost rigid NiO$_6$ octahedra. Tilt angles are of the order of a few degrees and depend on temperature and doping. It is convenient to index all phases on the basis of the $\sqrt{2}a \times \sqrt{2}b \times c$ supercell, relative to the parent K$_2$NiF$_4$ cell. Its lattice constants a and b and crystallographic directions are indicated in Fig. 3(a). In this supercell the interstitial O^{2-} ions reside at positions near $(\frac{1}{4}, \frac{1}{4}, \frac{1}{4})$, i.e., centered within the positive (La,Sr)O bilayers.[14] In the HTT phase ($F4/mmm$) the average octahedral tilt angle is zero [Fig. 3(a)]. This means that the NiO$_2$ planes are either flat or there is at least no coherent tilt pattern. Short-range correlations of
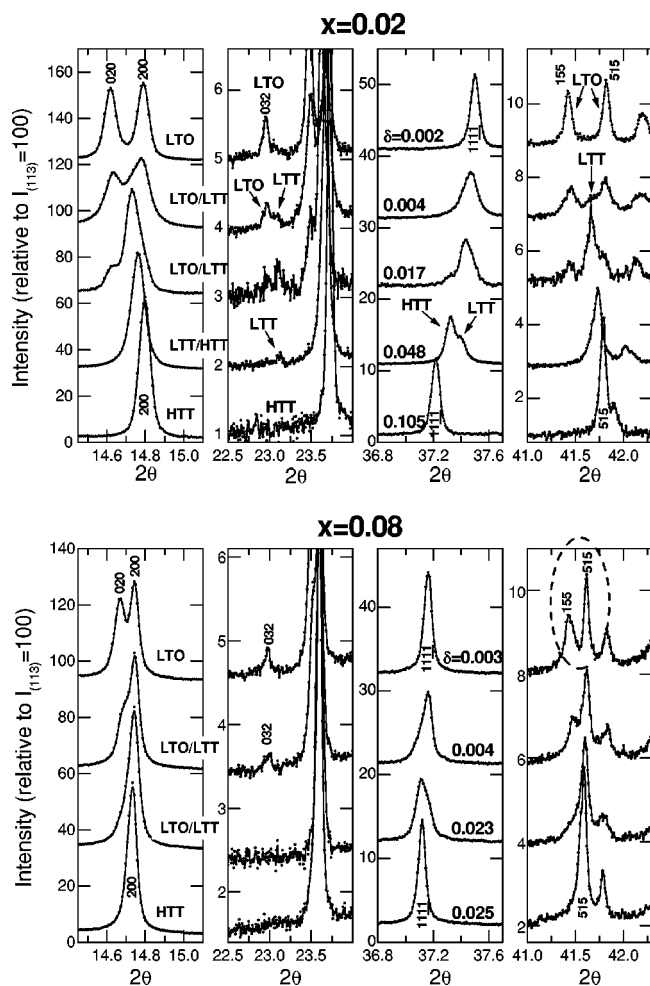
FIG. 4. Room-temperature diffraction patterns of La$_{2-x}$Sr$_x$NiO$_{4+\delta}$ for fixed Sr content $x=0.02$ and 0.08 and variable excess oxygen content δ.

octahedral tilts may exist due to local lattice distortion associated with O and Sr dopants. In the LTO phase (*Bmab*), the octahedra tilt antiferrodistortively around the [100] direction [Fig. 3(b)]. In the LTT phase (*P4$_2$/ncm*) the octahedral tilt axis is rotated in-plane by an azimuthal angle of 45° with respect to the LTO phase [Fig. 3(c)]. Since the direction of this rotation alternates in adjacent NiO$_2$ layers, tilt axes in adjacent layers are perpendicular to each other. Often the LTO2 phase (*Pccn*) is observed, which is an intermediate phase between the LTO and LTT phases, since the tilt axis is rotated by an angle $0° < \phi < 45°$. At very high δ an orthorhombic phase was reported for pure La$_2$NiO$_{4+\delta}$, for which the symmetry is *Fmmm*.[1,2,14] In the present study this phase was not observed, because in our Sr-doped samples δ is not high enough.

The powder diffraction patterns have been analyzed using the program Rietica to determine the lattice parameters.[40] The reflection conditions for the different phases are explained in Ref. 1. In the following, we focus on a few characteristic reflections (see Fig. 4) that are very helpful in distinguishing between the different phases and in determining phase fractions in the case of biphasic samples. The LTO phase manifests itself by a split of certain reflections with

$h \neq k$ such as (200)/(020) and (515)/(155). In addition, one observes superlattice reflections such as (212) or (032), which indicate coherent octahedral tilts. In the case of the LTT phase, the split for reflections with $h \neq k$ is absent, but the superlattice reflections (212) and (032) remain. Mixed LTO/LTT phases can be identified by the coexistence of split and nonsplit reflections as well as the presence of two of each of the superlattice reflections of (212) or (032), since the lattice constants of the LTO and LTT phases are different. Since the resolution at high angles is better than that at low angles, we have determined the LTO/LTT phase fractions from the (515)/(155) reflections. The HTT phase does not show any superlattice reflections; hence, the (212) and (032) reflections are absent. Mixed LTT/HTT phases are most readily identified by a split of reflections such as (008) and (11$\underline{11}$), as the c axis of the LTT and HTT phases are different. The c axis differs also for the LTO and LTT phases, but the difference is smaller and was not resolvable in our diffraction patterns. The LTO2 phase shows a similar but reduced orthorhombic splitting of the fundamental reflections as in the LTO phase as well as the superlattice reflections (122)/(212) and (302)/(032). It is well known that La$_2$NiO$_4$ at temperatures $T \lesssim 70$ K exhibits the LTO2 phase.[41] In our room temperature diffraction patterns, no evidence of the LTO2 phase was observed for any combination of x and δ.

Representative diffraction patterns for the different phases of samples with fixed Sr content $x=0.02$ and 0.08 are presented in Fig. 4 along with the δ values. For $x=0.02$ (top) the two miscibility gaps LTO/LTT and LTT/HTT were clearly detectable. Pure phases were observed only for the LTO and the HTT phase. A pure LTT phase was not detected, most probably because none of our prepared samples matched the required δ value. For $x=0.04$ and 0.06 we have in fact observed single-phase LTT samples. Due to the narrow δ range of the LTT phase it is generally difficult to obtain LTT-type samples, which also explains the small number of reports on this phase.

With increasing hole concentration, the structural differences between the LTO, LTT, and HTT phases generally decrease since the sublattice mismatch diminishes, making phase separations more difficult to detect. This is clearly the case for $x=0.08$ (bottom) where the orthorhombic strain in the stoichiometric sample ($\delta \simeq 0$) is already much weaker than for $x=0.02$ as one can see from the smaller splitting of the (155)/(515) reflections. With increasing δ we observed a mixed phase, but it was not possible to decide whether this phase is of the LTO/LTT or LTO/HTT type. Neither a pure LTT phase nor a mixed phase LTT/HTT was observed. Interestingly, for $x=0.08$ the (11$\underline{11}$) reflection of the biphasic samples show a significant asymmetry, indicating a majority LTO phase for $\delta=0.004$ and a majority LTT or HTT phase for $\delta=0.023$. Usually, LTO/LTT phase separation does not show up as clearly in a split of the (11$\underline{11}$) reflection as in the case of LTT/HTT phase separation. Therefore, the asymmetry of the (11$\underline{11}$) reflections for $x=0.08$ might indicate that the second phase is HTT. To solve this problem measurements at low temperatures are needed, where the tilt angles are larger.
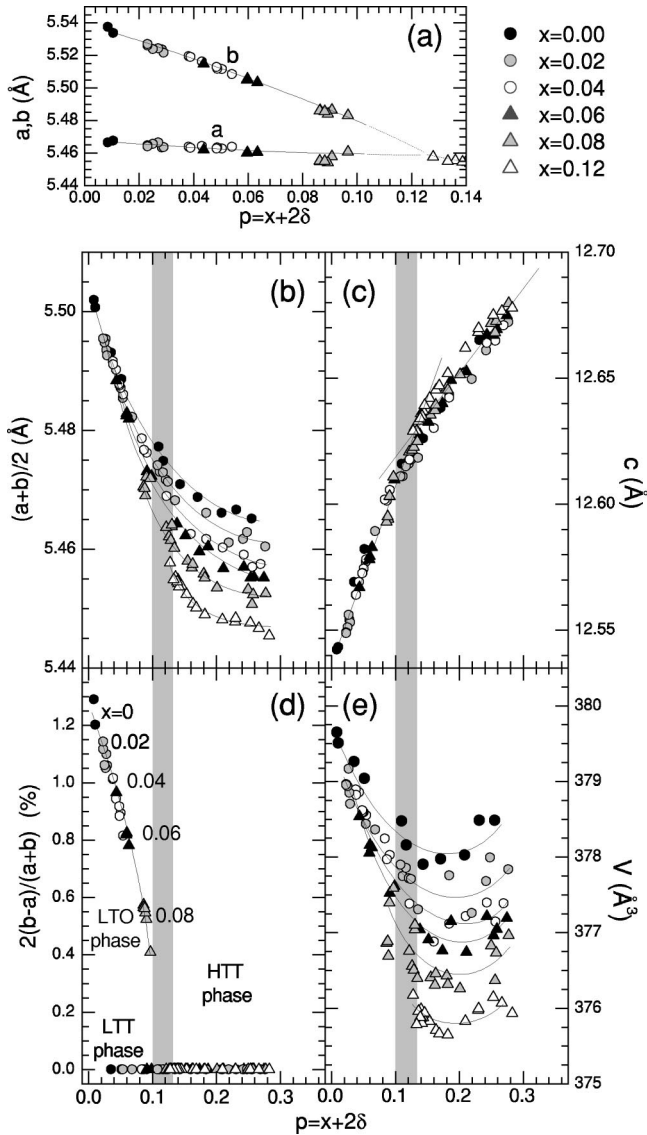
FIG. 5. Room-temperature lattice parameters a,b,c, unit cell volume V, and orthorhombic strain $2(b-a)/(a+b)$ of La$_{2-x}$Sr$_x$NiO$_{4+\delta}$ for fixed Sr content $x=0$, 0.02, 0.04, 0.06, 0.08, 0.12 and variable excess oxygen content δ as a function of hole content p. Solid lines are guides to the eye.

C. Lattice constants vs hole content $p=x+2\delta$

In Fig. 5 we show the lattice parameters as a function of the hole content $p=2x+\delta$. In this figure, only the data of single-phase samples or the majority phases of biphasic samples are included. [We have also created plots (not shown) of the lattice parameters as a function of $2c/(a+b)$ and the excess oxygen δ, but these provide no new insight.] In plot (b) we show the average basal plane lattice constant $(a+b)/2$ versus hole content. At low hole doping $p \lesssim 0.08$ the branches for the different sample series with fixed x almost coincide. In contrast, at higher hole doping the branches are clearly separated. The branch for the highest (lowest) Sr content shows the lowest (highest) values for $(a+b)/2$. All other branches for the various x values fill in systematically. A closer look at the lattice constants in the
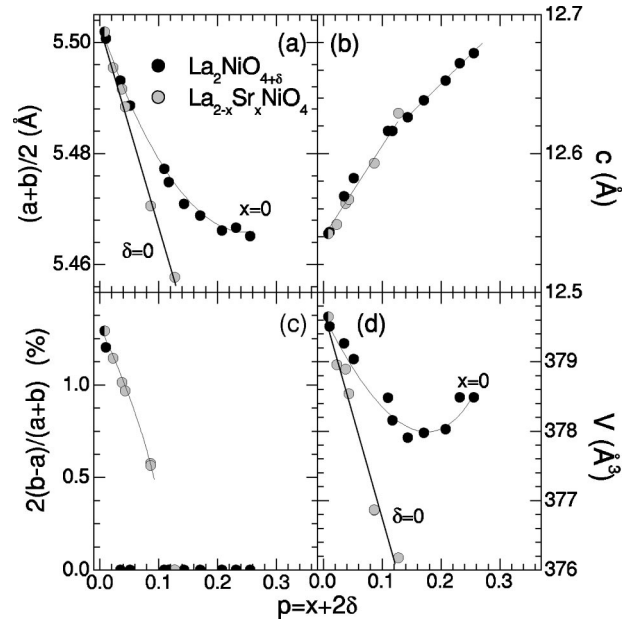
FIG. 6. Room-temperature lattice parameters $(a+b)/2$, c, $2(b-a)/(a+b)$, and V of La$_2$NiO$_4$ for pure Sr doping and pure O doping as a function of hole content p. Solid lines are guides to the eye.

LTO phase in Fig. 5(a) shows that a and b follow a nearly universal dependence on x and δ. Within each set of points having fixed x, the left most point has $\delta \simeq 0$, and then δ increases towards the right point. Accordingly, the orthorhombic strain also follows a universal curve as is shown in Fig. 5(d) where we plot the orthorhombic splitting in percent of $(a+b)/2$. With increasing p the splitting decreases and vanishes around $p=0.12$. Interestingly, the c-axis length shows a nearly unique dependence on p, as well [plot (c)]. As we will discuss later, that this is a coincidence is not obvious. In fact, it turns out that the c-axis length not only depends on p but also on the steric effects of the dopants. Furthermore, we observe a change in the slope dc/dp at around $p=0.12(2)$. At roughly this hole content, pure La$_{2-x}$Sr$_x$NiO$_4$ as a function of $p=x$ crosses over from LTO to HTT (at room temperature). Figure 5(e) shows the volume V of the supercell, which reveals no significant new insights. For fixed x the general trend is that, with increasing oxygen content, V first shrinks then saturates and eventually increases. Obviously V deviates from a linear dependence on oxygen doping, thereby violating Vegard's rule. Deviations from Vegard's rule are not uncommon among strongly anisotropic and/or nonstoichiometric crystal structures.[42,43]

1. Pure Sr doping vs pure O doping

The major differences between Sr and O doping become very clear when comparing the lattice parameters for pure Sr doping ($\delta=0$) and pure O doping ($x=0$). In Fig. 6 we show corresponding data as a function of p. For both types of hole doping, the average basal plane lattice constant $(a+b)/2$ decreases [plot (a)]. With increasing hole concentrations the oxygen-doped samples show significantly larger $(a+b)/2$ values as well as a tendency to saturate. For Sr doping $(a+b)/2$ decreases linearly, in agreement with Vegard's rule.
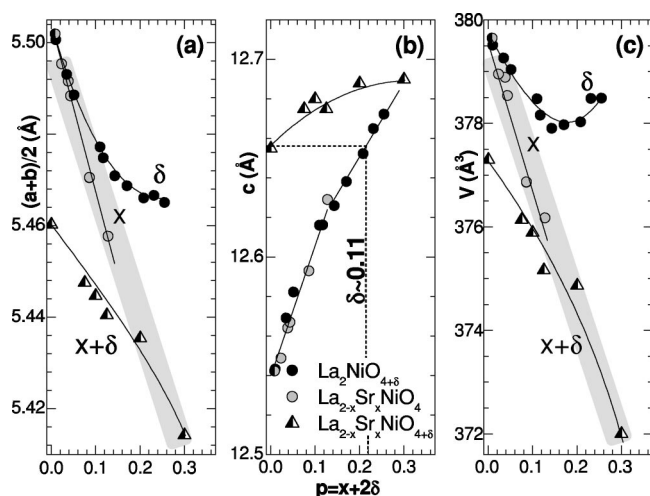
FIG. 7. Comparison of our lattice parameters for pure Sr and pure O doping with data for Sr-doped samples prepared in air (triangular symbols) taken from Ref. 32 at room temperature versus hole concentration. Solid lines are guides to the eye.

Since the dependence of c on x and δ is almost identical [plot 6(b)], the large differences observed for V are mainly due to the in-plane effects [plot 6(d)]. The differences clearly show that the lattice parameters do not solely depend on the hole content, but also on steric effects.

2. Comparison with as-prepared-in-air samples

In Fig. 7 we compare our results for pure Sr and pure O doping with the lattice parameters from Ref. 32 of Sr-doped samples prepared in air that were not post annealed. Air-prepared samples frequently contain a considerable amount of excess oxygen. From Fig. 7 it is apparent that this excess oxygen causes huge differences between the lattice parameters of annealed and air-prepared samples, particularly at low Sr concentrations. It is known that the excess oxygen concentration in air-prepared (not post-annealed) samples decreases with increasing Sr content, typically reaching $\delta \approx 0$ near $x=0.3$, and that for larger x oxygen vacancies are generated ($\delta < 0$). It is for this reason that in Fig. 7 the data points for pure Sr doping and those of the air-prepared samples for large $x \sim 0.3$ merge into a common Sr-doping dependence. From the lattice parameter c in Fig. 7(b) we estimate for the air-prepared sample with $x=0$ an excess oxygen content as high as $\delta \sim 0.11$.

D. Sr and O codoping phase diagrams

In Fig. 8 we present the individual oxygen-content phase diagrams for the various fixed Sr concentrations x with regard to the lattice parameters a and b. All data points stem from single-phase samples or the majority phase of biphasic samples. Biphasic samples with a pronounced majority phase are particularly useful for the determination of the delta value of the phase boundaries between the pure phases and the miscibility gaps. In Fig. 8 pure phases are represented by shaded areas and miscibility gaps by white areas. The hatched areas were not covered in this study. As one can see,
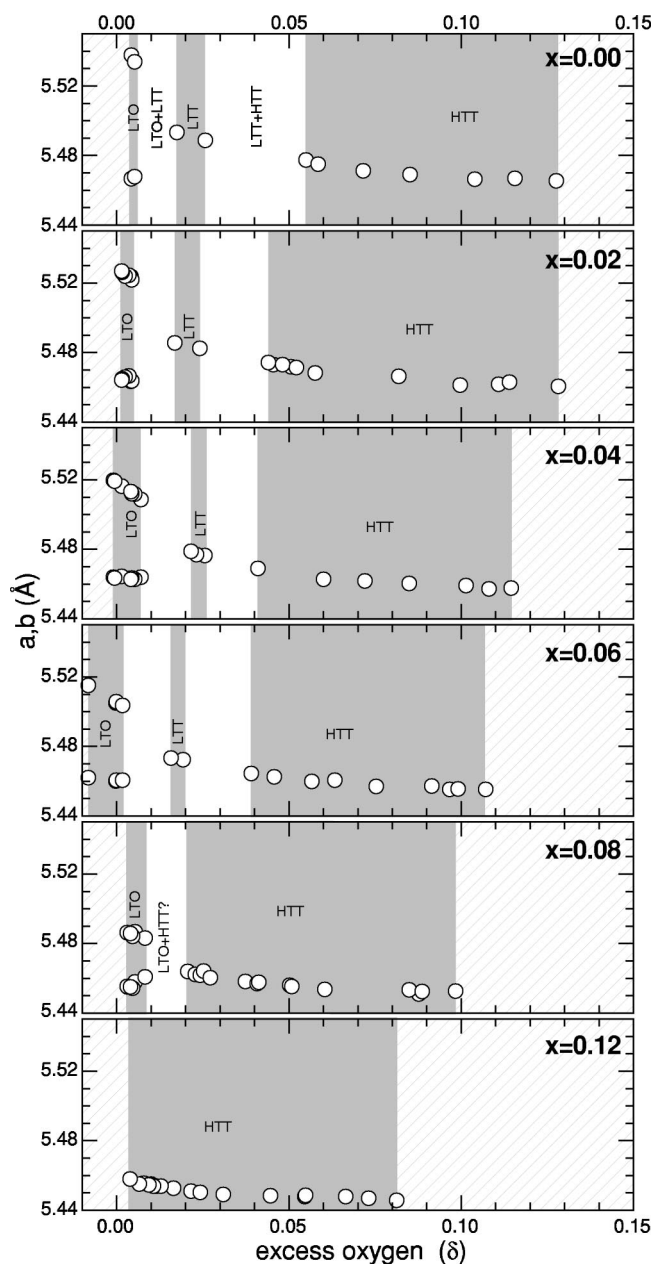
FIG. 8. Oxygen-content phase diagram for lattice parameters a and b of La$_{2-x}$Sr$_x$NiO$_{4+\delta}$ at room temperature for various Sr content x.

the maximum δ values obtained by anneals at 450 °C in O$_2$, systematically decrease with increasing Sr content. On the other hand, the lowest δ values scatter around $\delta \approx 0$ within the experimental error. In fact we assume that the most reduced samples are all very close to $\delta=0$. Note also, that the lattice parameters for $x=0$ and $\delta \leqslant 0.055$ were taken from our earlier publication in Ref. 1, but were refit according to Sec. III A. Hence, minor systematic differences between the phase diagram for $x=0$ in Fig. 8 and those in Fig. 1(b) and Ref. 1 are due to the fit procedure we have applied to all data sets (see Fig. 2). For $x=0$ one can clearly see the sequence of the pure LTO, LTT, and HTT phases, as well as the mixed LTO/LTT and LTT/HTT phases for intermediate δ values. The phase diagrams for $x=0.02$, 0.04, and 0.06 are qualita-

tively similar, but become increasingly difficult to resolve. According to our data, the δ range of the LTO phase slightly broadens from $x=0$ to $x=0.06$, while the LTT phase narrows. The pure LTO phase at room temperature never exists at δ values higher than 0.01. This means that δ has to be much smaller than 0.01 to be able to observe the intrinsic properties of La$_{2-x}$Sr$_x$NiO$_4$. The LTT phase is centered at about $\delta=0.02$, while the low δ phase boundary of the HTT phase systematically shifts to lower δ values.

Drastic changes of the phase diagram are observed for $x \geq 0.08$. For $x=0.08$ we were not able to detect the pure LTT phase, nor the second miscibility gap. Moreover, the δ range of the LTO phase again becomes narrower. To confirm these results we have prepared a second series of samples with $x=0.08$ which showed essentially the same behavior. At the end of Sec. III B we argue that for $x=0.08$ the first miscibility gap might be of the LTO/HTT type rather than LTO/LTT. Measurements at low temperatures where the octahedral tilts are larger, are needed to verify this result. For $x=0.12$ all samples are in the HTT phase. Only the most reduced samples show traces of the LTO phase and measurements at low temperatures reveal that these samples are indeed close to the HTT/LTO transition which occurs at about 275 K. In conclusion, our results for $x \geq 0.08$ clearly indicate a suppression of oxygen phase separation. Possible reasons will be discussed below. Finally, we emphasize that we do not observe any evidence for staging order or 3D interstitial order at room temperature.[4,27]

IV. DISCUSSION

Our experiments have revealed several key results. First of all, all Sr-doped samples in general should be assumed to be codoped unless their oxygen content was determined to be $\delta=0$. Furthermore, our results show that one has to clearly distinguish between Sr and O doping at any level of x, δ codoping. As long as miscibility gaps appear, their δ ranges depend mainly on the amount of excess oxygen and not on the hole content. Other features, such as the orthorhombic strain $2(b-a)/(a+b)$ and the c lattice parameter depend mainly on the hole content $p=x+2\delta$, independent of whether holes were introduced by Sr or O doping. In contrast, the average basal plane lattice constant $(a+b)/2$ (and, therefore, also the unit cell volume) depends explicitly on the individual concentrations of Sr and O.

A. Oxygen-content phase diagrams

The microscopic mechanism of phase separation and the concomitant structural transitions is quite complex and not fully explored. The fact that the doubly charged oxide interstitials are located within the positively charged rocksalt bilayers is consistent with the electrostatic environment. We assume that phase separation into oxygen-poor and -rich domains takes place by diffusion of the interstitials parallel to the rocksalt layers. Diffusion along the c axis is assumed to be negligible. [The diffusion process seems to be driven by the free energy $(\bar{G}_0)$ rather than by self-diffusion.[44]] The final ground state is a delicate balance between lattice distortions,

Coulomb repulsion between the interstitial O^{2-} ions, and screening effects by the charge carriers in the NiO$_2$ planes. With increasing δ, the LTT phase becomes energetically favorable over the LTO phase, though the stabilization of the initial LTT domains requires a minimum concentration of interstitials. Within the first miscibility gap it is obviously energetically favorable for the interstitials to separate into oxygen-poor LTO and oxygen-rich LTT domains, i.e., the overall gain in lattice distortion energy by forming O^{2-} depleted LTO as well as O^{2-} enriched LTT domains compensates the loss in Coulomb energy due to the enhanced charge inhomogeneity in the rocksalt layers and possibly also in the NiO$_2$ planes. Evidence for a charge inhomogeneity in the NiO$_2$ planes at this low level of O doping comes from studies of the magnetic properties, which indicate the coexistence of domains with Néel temperatures typical for the pure phases, i.e., the coexistence of domains with different hole concentrations.[4,45] This is very similar to La$_2$CuO$_{4+\delta}$ where phase separation results in superconducting and antiferromagnetic domains,[46] indicating not only the formation of oxygen-rich and -poor domains, but also a corresponding charge inhomogeneity in the CuO$_2$ planes.

The LTT phase exists only in a very narrow range of δ. At higher δ the room-temperature structure eventually becomes HTT. The HTT phase is characterized by a disordered noncoherent octahedral tilt pattern. There are certainly several factors responsible for the doping-dependent crossover from the LTT to the HTT phase. We assume that in HTT domains the reduction of the sublattice mismatch with increasing hole concentration has advanced to such a degree that no coherent tilt pattern is possible. The observation of orthorhombic staged phases at temperatures slightly below room temperature show that, in principle, a phase with a coherent tilt pattern can be induced at high hole and oxygen concentrations, as well.

Structural models proposed in Ref. 4 suggest that the LTT structure is indeed more suitable for accommodation of the interstitials than the LTO phase. However, the concentration of excess oxygen is not the only parameter that determines the phase diagram. In Pr$_2$NiO$_{4+\delta}$, for example, the δ range of the pure LTT phase is centered at $\delta \simeq 0.06$ in contrast to $\delta \simeq 0.02$ in La$_2$NiO$_{4+\delta}$ (see Fig. 9).[33,47] Moreover, no HTT phase is observed between the LTT and the orthorhombic high-δ phase (*Fmmm*). Since trivalent Pr is smaller than La, in Pr$_2$NiO$_4$ the sublattice mismatch is larger, i.e., the octahedral tilt angle is larger and the c axis shorter.[33,47] The change of the local environment of the interstitial site obviously makes it more difficult to stabilize the LTT phase. It is worth mentioning that in a Pr-based sample, annealed under identical conditions as a La-based sample, the interstitial oxygen content is higher.

So far, we have considered the effects of oxygen doping. Additional doping with Sr, on one hand, introduces random lattice defects and, on the other hand, Coulomb repulsion between the relatively negative (compared to La) Sr sites and the O interstitials. Furthermore, Sr doping increases the concentration of holes. The holes in the NiO$_2$ planes might be expected to screen the O^{2-} interstitials, as well as the Sr impurities in the rocksalt layers, which should result in a reduced O-O and Sr-O Coulomb repulsion. From our results,
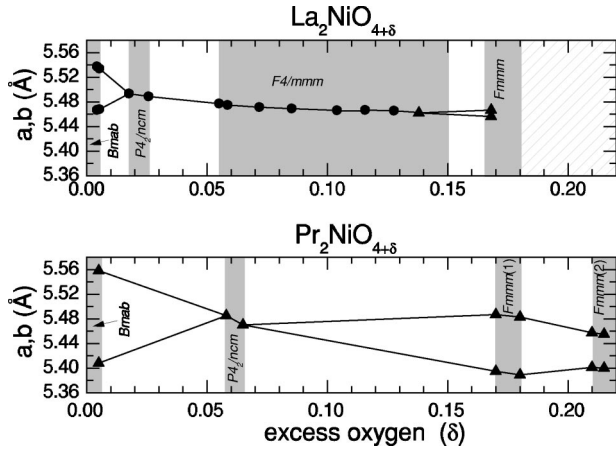
FIG. 9. Oxygen-content phase diagrams for lattice parameters a and b of La_2NiO_4 (solid triangles taken from Ref. 1) and Pr_2NiO_4 (after Ref. 33) at room temperature.

however, we have obtained no evidence that screening has a significant impact on the oxygen interstitials. On the other hand, our data yield clear signatures of an influence of Sr doping on the oxygen-content phase diagram: the suppression of oxygen phase separation for $x \geq 0.08$ as well as a weak change of the widths of the LTO and LTT phases for $x \leq 0.06$.

One possible explanation is that the Coulomb interaction between the O interstitials and Sr defects suppresses the tendency for phase separation into oxygen-rich and oxygen-poor domains. However, other factors can also cause the observed changes. As our comparison with $Pr_2NiO_{4+\delta}$ has shown, it might well be that with decreasing octahedral tilt angle (with increasing x) the phase boundaries shift in δ as well as in temperature. Since the miscibility gap boundaries near the upper consolutes are rounded, the δ range of the gap depends on the temperature of the experiment relative to the upper consolute temperature. This can explain a broadening or narrowing of the pure phases, too. In this context, the successive disappearance of the miscibility gaps for $x \geq 0.08$ can occur if their upper consolute temperatures drop below room temperature.

We note that, though the structural differences between the LTO, LTT, and HTT phases decrease with increasing Sr concentration, oxygen phase separation, in principle, should stay detectable. Even in the extreme case of a phase separation into oxygen-rich and oxygen-poor HTT domains, the lattice parameters of these two HTT phases would be different and therefore distinguishable. As we have no indication that this happens in our samples with $x \geq 0.08$, we assume that we have indeed observed a suppression of the phase separation, as mentioned above. Further measurements at variable T to track the consolute temperature as a function of x and δ, as well as at low T where the lattice distortions are usually larger, are necessary to confirm this point.

B. Structural anisotropy

In Fig. 10 we compare our results for the lattice parameters of $La_{2-x}Sr_xNiO_{4+\delta}$ with data for Ba-, Sr-, and Ca-doped
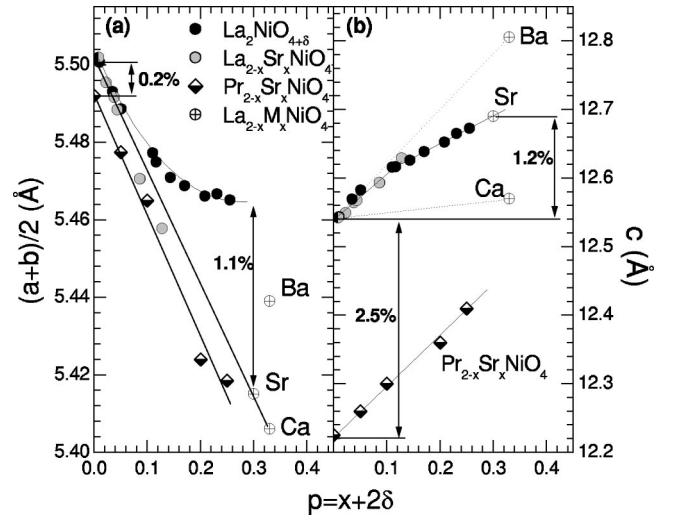
FIG. 10. Room-temperature lattice parameters $(a+b)/2$ (left) and c (right) for doped La_2NiO_4 and Pr_2NiO_4 as a function of hole content p. Data for $La_{2-x}M_xNiO_4$ with $M =$ Ca, Sr, and Ba ($\oplus$) was taken from Ref. 32, and references cited therein. Data for $Pr_{2-x}Sr_xNiO_4$ was taken from Ref. 34. Solid and dotted lines are guides to the eye.

La_2NiO_4 from Ref. 32, and references cited therein, as well as Pr_2NiO_4 from Ref. 34. Note that in Ref. 32 a broad Sr range was covered ($0 \leq x \leq 1$). We limit our comparison to $x \sim 0.3$ since only around this Sr content does one obtain $\delta \simeq 0$ in typical air-prepared samples (Sec. III C 2). We assume a similar situation for Ca and Ba doping. Let us focus first on the behavior of c in Fig. 10(b). The coincidence of our data for La_2NiO_4 for pure O doping and pure Sr doping up to $x = 0.12$ is confirmed by a point at $x = 0.3$ taken from Ref. 32. In contrast, c is significantly larger for a Ba-doped sample and shorter for a Ca-doped sample, both with $x = 0.33$. In the case of Pr_2NiO_4 the c axis is about 2.5% shorter than in La_2NiO_4, but it shows a similar Sr-doping dependence as La_2NiO_4 at low $x \leq 0.12$. A comparison of the ionic radii of the substituting elements shows that c qualitatively scales with the average ionic radii at the La site: $Ba^{2+}:Sr^{2+}:La^{3+}:Ca^{2+}:Pr^{3+} \Rightarrow 1.47$ Å$:1.31$ Å$:1.216$ Å$:1.18$ Å$:1.179$ Å.[48] Therefore, we conclude that the coincidence of c for Sr- and O-doped La_2NiO_4 is coincidental.

As shown in Fig. 10(a), out of all dopants, interstitial oxygen shows the largest in-plane lattice constants. Even for Ba, the largest dopant, $(a+b)/2$ stays significantly smaller than for oxygen doping. We assume that this is due to a large chemical pressure of the intercalated oxygen ions. Interestingly, the Ca-doped sample is in line with the Sr data, and the data for $Pr_{2-x}Sr_xNiO_4$ are just 0.2% lower than for $La_{2-x}Sr_xNiO_4$. The fact that, compared to c, $(a+b)/2$ barely depends on the average ionic radii at the La site shows that the chemical pressure for La site doping is highly anisotropic. Furthermore, we have to conclude that the decrease of $(a+b)/2$ upon Sr doping is largely due to the dependence of the Ni-O bond length upon hole doping. If this conclusion is correct, then the much weaker decrease of $(a+b)/2$ observed for oxygen doping effectively indicates an expansion of the ab plane by oxygen interstitials. At a hole content of p

$\simeq 0.3$, this expansion amounts to $\sim 1.1\%$ which has to be compared to an expansion of the c axis by 1.2% (see Fig. 10). Therefore, we conclude that interstitial oxygens cause an almost isotropic expansion. We note furthermore, that a strongly anisotropic lattice expansion has also been observed in the LTO phase of Nd-doped La$_{2-x}$Sr$_x$CuO$_4$.[49]

Finally we discuss the change of the slope dc/dp in Fig. 5(c) at a hole content of $p \simeq 0.12$. This effect was also observed by Tamura *et al.* in La$_2$NiO$_{4+\delta}$ with $x=0$.[2] There are certainly several factors that contribute to the Sr- and O-doping dependence of c. One factor is the chemical pressure of the dopants, as was discussed above. Next, hole doping leads to a decrease of the sublattice mismatch, which causes the NiO$_6$ octahedra to straighten up. This results in an increase of c, and further is an additional reason for the stabilization of the HTT phase. On the other hand, O and Sr doping lead to significant disorder within the octahedral tilts, because the surrounding apical oxygens are pushed away from the defect site (even in the HTT phase). Tilt disorder, therefore, effectively causes c to decrease. Furthermore, it is assumed that the accompanying disruption of the coherent tilt pattern stabilizes the HTT phase, as well. A closer look at Fig. 5(c) shows that the slope dc/dp becomes smaller at approximately the hole content where the samples enter the pure HTT phase. At the moment we cannot conclusively say whether this effect represents a distinct crossover or a gradual variation. However, one possible explanation involves the already mentioned contribution coming from a change of the octahedral tilt angle for the coherent tilt pattern. This contribution is zero in the HTT phase and therefore might cause the slower increase of c with increasing p. We mention that in La$_{1.95}$Bi$_{0.05}$CuO$_{4+\delta}$, as well, a change of $dc/d\delta$ at $\delta \simeq 0.07$ was observed.[50] In La$_{2-x}$Sr$_x$CuO$_4$, a similar behavior might be related to an increasing concentration of oxygen vacancies for $x \gtrsim 0.25$.[51] Nevertheless, in this compound the feature occurs roughly at the Sr-doping-dependent crossover from the LTO phase to the HTT phase, as well.

V. CONCLUSION

In summary, we have presented a detailed x-ray powder diffraction study of Sr- and O-codoped La$_2$NiO$_4$ at room temperature. From the lattice parameters we have constructed the oxygen-content phase diagram for each investigated Sr content. At low Sr concentrations $x \leq 0.06$ the phase diagrams are qualitatively similar to that for $x=0$. However, significant changes occur for $x \geq 0.08$ where phase separation progressively disappears. We have argued that both the Coulomb interaction between the oxygen interstitials and the Sr defects, and the reduction of the octahedral tilt angle by Sr doping contribute to this effect. A comparison of the lattice parameters of codoped samples reveals that one has to clearly distinguish between Sr and O doping. Furthermore, we have systematically characterized the differences between pure Sr and pure O doping, as well as Sr-doped samples prepared in air. A comparison with other dopants shows that the chemical pressure of the La site dopants is strongly anisotropic, while oxygen interstitials exhibit a more isotropic chemical pressure.

One particularly useful finding from this study is, that oxygen interstitial concentrations in excess of $\delta \cong 0.01$ will all lead to phase separation (for x up to at least 0.08). Hence, an investigation of the intrinsic properties of La$_{2-x}$Sr$_x$NiO$_4$ requires that $\delta \ll 0.01$. Finally, this study provides a (x,δ)-structure map which can be used to determine the oxygen content of a Sr-doped sample with $x \leq 0.12$ by measuring the x-ray powder diffraction pattern.

ACKNOWLEDGMENTS

[1] D. E. Rice and D. J. Buttrey, J. Solid State Chem. **105**, 197 (1993).

[2] H. Tamura, A. Hayashi, and Y. Ueda, Physica C **216**, 83 (1993).

[3] J. M. Tranquada, in *Neutron Scattering in Layered Copper-Oxide Superconductors*, edited by A. Furrer (Kluwer, Dordrecht, 1998), p. 225.

[4] J. M. Tranquada, Y. Kong, J. E. Lorenzo, D. J. Buttrey, D. E. Rice, and V. Sachan, Phys. Rev. B **50**, 6340 (1994).

[5] P. G. Radaelli, J. D. Jorgensen, R. Kleb, B. A. Hunter, F. C. Chou, and D. C. Johnston, Phys. Rev. B **49**, 6239 (1994).

[6] B. O. Wells, Y. S. Lee, M. A. Kastner, R. J. Christianson, R. J. Birgeneau, K. Yamada, Y. Endoh, and G. Shirane, Science **277**, 1067 (1997).

[7] M. A. Kastner and R. J. Birgeneau, Rev. Mod. Phys. **70**, 897 (1998).

[8] B. O. Wells, R. J. Birgeneau, F. C. Chou, Y. Endoh, D. C. Johnston, M. A. Kastner, Y. S. Lee, G. Shirane, J. M. Tranquada, and K. Yamada, Z. Phys. B: Condens. Matter **100**, 535 (1996).

[9] B. Khaykovich, R. J. Birgeneau, F. C. Chou, R. W. Erwin, and M. A. Kastner, Phys. Rev. B **67**, 054501 (2003).

[10] F. C. Chou, D. C. Johnston, S.-W. Cheong, and P. C. Canfield, Physica C **216**, 66 (1993).

[11] J. M. Tranquada, Ferroelectrics **177**, 43 (1996).

[12] J. M. Tranquada, B. J. Sternlieb, J. D. Axe, Y. Nakamura, and S. Uchida, Nature (London) **375**, 561 (1995).

[13] The designation "LTT" is commonly used for the low-temperature phase with spacegroup $P4_2/ncm$ in La$_{2-x}$Sr$_x$CuO$_4$ and La$_{2-x}$Sr$_x$NiO$_4$. Therefore, we also use this designation for the $P4_2/ncm$ phase of the oxygen-content phase diagram, though in this case the LTT phase is not restricted to low temperatures.

[14] J. D. Jorgensen, B. Dabrowski, S. Pei, D. R. Richards, and D. G.

Hinks, Phys. Rev. B **40**, 2187 (1989).

[15] H. Tamura, A. Hayashi, and Y. Ueda, Physica C **258**, 61 (1996).

[16] M. Medarde and J. Rodríguez-Carvajal, Z. Phys. B: Condens. Matter **102**, 307 (1997).

[17] N. J. Poirot, P. Odier, and P. Simon, J. Alloys Compd. **262–263**, 147 (1997).

[18] N. J. Poirot, P. Simon, P. Odier, and J. M. Bassat, Eur. Phys. J. B **2**, 469 (1998).

[19] S. M. Hayden, G. H. Lander, J. Zarestky, P. J. Brown, C. Stassis, P. Metcalf, and J. M. Honig, Phys. Rev. Lett. **68**, 1061 (1992).

[20] V. Sachan, D. J. Buttrey, J. M. Tranquada, J. E. Lorenzo, and G. Shirane, Phys. Rev. B **51**, 12 742 (1995).

[21] O. Friedt, diploma thesis 1998, University of Cologne, Germany.

[22] J. M. Tranquada, D. J. Buttrey, and V. Sachan, Phys. Rev. B **54**, 12 318 (1996).

[23] P. Wochner, J. M. Tranquada, D. J. Buttrey, and V. Sachan, Phys. Rev. B **57**, 1066 (1998).

[24] C. C. Homes, J. M. Tranquada, Q. Li, A. R. Moodenbaugh, and D. J. Buttrey, Phys. Rev. B **67**, 184516 (2003).

[25] Z. Hiroi, T. Obata, M. Takano, Y. Bando, Y. Takeda, and O. Yamamoto, Phys. Rev. B **41**, 11 665 (1990).

[26] C. H. Chen, S-W. Cheong, and A. S. Cooper, Phys. Rev. Lett. **71**, 2461 (1993).

[27] J. M. Tranquada, J. E. Lorenzo, D. J. Buttrey, and V. Sachan, Phys. Rev. B **52**, 3581 (1995).

[28] J. Rodríguez-Carvajal, M. T. Fernández-Díaz, and J. L. Martínez, J. Phys.: Condens. Matter **3**, 3215 (1991).

[29] K. Nakajima, K. Yamada, S. Hosoya, Y. Endoh, M. Greven, and R. J. Birgeneau, Z. Phys. B: Condens. Matter **96**, 479 (1995).

[30] J. M. Tranquada, D. J. Buttrey, V. Sachan, and J. E. Lorenzo, Phys. Rev. Lett. **73**, 1003 (1994).

[31] In this work the oxygen fugacity corresponds approximately to the oxygen partial pressure, due to the low value of pressure.

[32] S. H. Han, M. B. Maple, Z. Fisk, S-W. Cheong, A. S. Cooper, O. Chmaissem, J. D. Sullivan, and M. Marezio, Phys. Rev. B **52**, 1347 (1995).

[33] J. D. Sullivan, D. J. Buttrey, D. E. Cox, and J. Hriljac, J. Solid State Chem. **94**, 337 (1991).

[34] J. D. Sullivan, Ph.D. thesis, University of Delaware, 1992.

[35] D. J. Buttrey, H. R. Harrison, J. M. Honig, and R. R. Schartman, J. Solid State Chem. **54**, 407 (1984).

[36] D. J. Buttrey and J. M. Honig, in *The Chemistry of High Temperature Superconductors*, edited by C. N. R. Rao (World Scientific, Singapore, 1991), pp. 283–305.

[37] D. J. Buttrey, V. Sachan, J. M. Tranquada, and J. E. Lorenzo, in *Proceedings of the Seventh Annual Symposium on Superconductivity*, edited by K. Yamafuji and T. Morishita (Springer Verlag, Berlin, 1994).

[38] D. J. Buttrey, in *Perspectives in Solid State Chemistry*, edited by K. J. Rao (Narosa Publishing House, New Delhi, 1995), pp. 228–240.

[39] G. C. Smith, Oil Gas Investor **4**, 24 (1991).

[40] B. Hunter, RIETICA–A visual Rietveld program (unpublished).

[41] J. Rodríguez-Carvajal, J. L. Martínez, J. Pannetier, and R. Saez-Puche, Phys. Rev. B **38**, 7148 (1988).

[42] S. Lee, H. Miyazaki, S. D. Mahanti, and S. A. Solin, Phys. Rev. Lett. **62**, 3066 (1989).

[43] P. Ganguly, N. Shah, M. Phadke, V. Ramaswamy, and I. S. Mulla, Phys. Rev. B **47**, 991 (1993).

[44] A. Jacobson (private communication).

[45] S. Hosoya, T. Omata, K. Nakajima, K. Yamada, and Y. Endoh, Physica C **202**, 188 (1992).

[46] J. H. Cho, F. C. Chou, and D. C. Johnston, Phys. Rev. Lett. **70**, 222 (1993).

[47] D. J. Buttrey, J. D. Sullivan, G. Shirane, and K. Yamada, Phys. Rev. B **42**, 3944 (1990).

[48] R. D. Shannon, Acta Crystallogr., Sect. A: Cryst. Phys., Diffr., Theor. Gen. Crystallogr. **32**, 751 (1976).

[49] B. Büchner, Ph.D. thesis, University of Cologne, Germany, 1994.

[50] M. Kato, H. Chizawa, Y. Ono, and Y. Koike, Physica C **256**, 253 (1996).

[51] P. G. Radaelli, D. G. Hinks, A. W. Mitchell, B. A. Hunter, J. L. Wagner, B. Dabrowski, K. G. Vandervoort, H. K. Viswanathan, and J. D. Jorgensen, Phys. Rev. B **49**, 4163 (1994).